Simulation of Migrative Excitation Trapping in Aromatic Chains with Nonrandom Site Disorder: Trap Location, Fluorescence, and Detrapping

Bernhard Mollay and Harald F. Kauffmann*

Institut für Physikalische Chemie der Universität Wien, Währingerstrasse 42, A-1090 Wien, Austria

Received December 15, 1993; Revised Manuscript Received May 17, 1994•

ABSTRACT: A simulation is presented that microscopically accounts for the role of incoherent excitation transfer in immobile, nonrandom pendent group aromatic polymers (single chain limit). By using a Monte-Carlo standard routine and master equation simulation software, accurate statistical mechanical averages of the relaxing optical excitation have been calculated for self-avoiding random chains of length $N = 50$ and $N = 100$ (50 and 100 sites). Both the frequency-regime solution and its time-domain analog, i.e. the eigenvalues spectrum $\langle\Phi(\omega_i)\rangle$ and the excitation survival propability $\langle p(t)\rangle$, respectively, have been computed. The focus of the simulations has been the study of excitation trapping as a function of varying D–D intersite coupling (i) for different trap locations (end-tagged vs random) and dimensionality, (ii) in presence of a radiative cutoff (fluorescence), and (iii) for reversible D–T events (detrapping) due to thermal release. We show that, in particular, the frequency spectrum of hopping modes $\langle\Phi(\omega_i)\rangle$ represents a powerful tool for extracting dynamical information that is usually concealed in phenomenological (nonexponential) kinetic models. The importance of reconstructing $\langle\Phi(\omega_i)\rangle$ from fluorescence convolution data by means of unbiased, numerical inversion in future measurements has been addressed.

I. Introduction

In an aromatic polymer with the main chain built up by the σ-bonds of a carbon skeleton the ensemble of aromatic sites in conjunction with the manifold of chain conformations induces a multitude of molecular arrangements and, thus, significantly positional disorder of the aromatic sites, the fluctuations being controlled by the aromatic site density, the dimension of the molecular polymer array, and the statistical chain parameters.[1] Upon optical excitation the array of individual molecular absorbers (sites) creates a distribution of localized S_1-states (weak coupling limit) that (i) reflects the molecular site disorder and (ii) controls electronic intersite interaction for both transport and trapping.[2,3] For phonon temperatures not too low, a migrating molecular excitation in an aromatic polymer is generally assumed to spend part of its life as a hopping exciton where the phase memory of the excitation is lost and the temporal evolution obeys predominantly incoherent dynamics.[4]

The role of spatial disorder on the dynamics of incoherent excitation transfer and its effect on the transient fluorescence pattern in finite-sized aromatic polymers is a formidable theoretical problem.[5] The analytical treatment of the (ensemble-averaged) *donor survival function*, $\langle p(t)\rangle$, important in the analysis of a transient polymer fluorescence experiment, has to be restricted to polymers for which the aromatic groups (donor sites) are energetically equivalent and distributed *randomly* (low site-density regime). On these premises Laplace-domain approaches to the transport master equation were developed[6,7] and the first connection was made to polymer fluorescence data.[8] More recently, appropriate time-domain Green function solutions based on the two-body cumulant expansion[9] were obtained by Fayer's group[10] that allowed, under favorable conditions, polymer conformation to be probed in fluorescence depolarization measurements.[11]

However, many realistic aromatic polymers fall into the high-density limit where the aromatic sites are distributed in a *nonrandom* fashion for the majority of morphological situations. A typical example is the pathological site topology of aromatic *vinyl homopolymers* in which the aromatic sites are bound to the carbon chain skeleton in a 1,3-sequence; i.e. their distribution is neither random nor periodic. As a result, no analytical site-to-site pair correlation function $S(\mathbf{R})$ is available that would allow the construction of closed-form statistical-mechanical averages for the donor survival function. A unified treatment of the optical dynamics continues, therefore, to be an elusive problem in these systems.

The present work is an effort toward disentangling the many-body dynamics caused by transport, trapping, and nonrandom disorder in a pendent group aromatic polymer by applying a computer simulation. The technique which we employ here combines a Monte-Carlo chain generation and a master equation diagonalization algorithm for the computation of the chain excitation dynamics.[12,13] Our computational scheme interrogates the frequency domain solutions, i.e. the exact eigenvalues spectrum $\langle\Phi(\omega_i)\rangle$, in a first step, and thus differs from the methodology given by Byers et al.[14,15] who used the recursive residue generation method (RRGM) Lanczos tridiagonalization[16] without solving the eigenvalue problem of the high-dimensional relaxation matrix.

The particular photophysical problem we will address is the scattering of a statistical molecular site excitation in an ensemble of static, polymer-bound, aromatic sites that show spatial (off-diagonal), *nonrandom* disorder. Our analyses will focus on typical *migrative trapping* experiments with the objective of calculating the statistical mechanical averages of frequency- and time-domain solutions for both donor and trap, directly related to the δ-pulse fluorescence response of the polymer. What we wish to demonstrate here is the typical kinetic signature of migrational trapping for a selection of polymer-topological situations and photophysical variations. For iso-energetic sites and irreversible trapping the cases to be presented include (i) the role of trap position (end-tagged vs random) in a 1-D chain calculated for various donor–donor (D–D) coupling-strengths, (ii) the influence of chain dimension for a fixed trap location, and (iii) the

* To whom correspondence should be addressed.

• Abstract published in *Advance ACS Abstracts*, July 15, 1994. *Polym. Prepr. (Am. Chem. Soc., Div. Polym. Chem.)* **1992**, *33*, 72.

0024-9297/94/2227-5129$04.50/0

effect of a radiative deactivation channel (fluorescence) on the overall optical relaxation process. Another focus is the consequence of *reversible* constraints of traps due to thermal release (detrapping) and its effect on the fluorescence response of donor and trap, respectively. For all these scenarios the accurate calculation of the *eigenvalues spectrum* provides a powerful tool for probing different photophysical situations and transport topologies that helps one to develop a preliminary understanding of how pattern analysis of polymer fluorescence has to be devised.

II. Computational Technique and Polymer Model

As reported by us in previous work,[12] the simulation software combines (i) a static Monte-Carlo method (generations of chains) and (ii) a dynamical algorithm for solving the master equation. In this technique the coordinates of a single chain geometry have been synthesized by a simple self-avoiding random walk (SSAW) on quadratic and cubic lattices.[17] Typically, the chain consists of 50–100 sites (located at the intersections of the bond vectors) with a nearest-neighbor intersite separation that mimics the 1,3 head-to-tail configuration in an aromatic polymer. In one part of the work a single trap (49 donors, 1 trap) has been attached to the chain either in a *random* fashion or end-tagged to the chain. In other simulation runs a trap density $\rho_T = 0.1$ has been chosen (90 donor, 10 traps). The excitation dynamics along the polymer contour have then been modeled in terms of a master equation (next section) and numerically solved by a diagonalization routine.[18] For the moderate dimensions considered here (50–100 sites) the method yields exact solutions for arbitrary relaxation matrices **W**. In order to achieve a realistic statistical average of the ensemble and its dynamics, typically $N = 5000$–$10\,000$ chain configurations have been generated and superimposed. The important quantity computed in these simulations is the (configurationally averaged) *eigenvalues spectrum* of the hopping process $\langle \Phi(\omega_i) \rangle$ and, in a second step, the donor (or trap) survival function $\langle p(t) \rangle$ assembled via the Laplace transform. The theoretical description necessary to understand the simulation procedure is briefly given in the next section. For a detailed formulation of the statistical-mechanical background see ref 12.

III. Theoretical Formulation

For the incoherent motion of a single molecular excitation along energy-degenerate sites of a particular chain configuration the n-dimensional Pauli master equation has to be solved

$$\dot{\mathbf{p}}(t) = \mathbf{W}\mathbf{p}(t) \qquad \mathbf{W} = [W_{ij}]_{n\times n} \tag{III.1}$$

$\mathbf{p}(t)$ is the excitation column vector with components, $p_i(t)$ representing the site probability elements and **W** is the transition matrix with elements

$$W_{ij} = (1 - \delta_{ij})\gamma_{ji} - \delta_{ij}\left(\sum_{\substack{l=1 \\ l\neq i}}^{n} \gamma_{il} + k_i\right) \tag{III.2}$$

In eq III.2 δ_{ij} is the Kronecker delta. γ_{ji} and γ_{il} represent the rate constants for the transitions $j \rightarrow i$, $i \rightarrow l$, thus reflecting the individual gain and loss terms. The rate constants k_i refer to the finite fluorescence lifetime of the individual sites that contain donors ($k_i \doteq k_D$; $i = 1, ..., n_D$) and traps ($k_i \doteq k_T$; $i = n_D + 1, ..., n$).

According to the various degrees of freedom of interaction between donor–donor (D–D), donor–trap (D–T, trapping), and trap–donor (T–D, detrapping) the hopping rates for our system decompose into 3 groups:

$$\gamma_{ij} \doteq \begin{cases} \gamma_{ij}^{DD} & i, j = 1, ..., n_D \\ \gamma_{ij}^{DT} & i = 1, ..., n_D;\ j = n_D + 1, ..., n \\ \gamma_{ij}^{TD} & i = n_D + 1, ..., n;\ i = 1, ..., n_D \end{cases} \tag{III.3}$$

For the calculation of matrix elements the (isotropic) dipole–dipole coupling for D–D transfer has been assumed[19]

$$\gamma_{ij}^{DD} = \eta_0^{DD}\left(\frac{d^{DD}}{|r_i - r_j|}\right)^6 \tag{III.4}$$

with symmetric transition rates between sites i and j, $\gamma_{ij}^{DD} = \gamma_{ji}^{DD}$ (pure positional disorder). d^{DD} is the minimal site-to-site separation between donors and η_0^{DD} is the transfer rate when $r_i - r_j$ equals d^{DD} (maximum nearest-neighbor transition frequency). For simplicity, the same Förster-type expression has been considered for the trapping process (γ_{ij}^{DT}). All dipolar interactions have been taken into account in this analysis, so no cutoff has been used.

The general solution to eq III.1 is a linear combination of n independent solution vectors

$$\mathbf{p}(t) = \sum_{j=1}^{n} c_j \mathbf{p}_j(t) \tag{III.5}$$

with scalar c_j containing the initial excitation boundary condition. With the ansatz

$$\mathbf{p}_j(t) = \mathbf{v}_j e^{\lambda_j t} \qquad j = 1, ..., n \tag{III.6}$$

($\mathbf{v}_j$, eigenvector; λ_j, eigenvalue) one obtains

$$\mathbf{p}(t) = \sum_{j=1}^{n} c_j \mathbf{v}_j e^{\lambda_j t} \qquad j = 1, ..., n \tag{III.7}$$

or in terms of the fundamental matrix

$$\mathbf{p}(t) = \mathbf{Q}(t)\mathbf{c}$$

$$\mathbf{Q}(t) = [v_{ij} e^{\lambda_j t}]_{n\times n} \qquad j = 1, ..., n \tag{III.8}$$

v_{ij} being the elements of the transposed eigenvector $\mathbf{v}_j = (v_{1j}, ..., v_{nj})^T$. Combining eq III.6 with eq III.1 the matrix equation for the eigenvalue problem reads

$$[\mathbf{W} - \lambda_j \mathbf{I}]\ \mathbf{v}_j = \mathbf{0} \tag{III.9}$$

with identity matrix $\mathbf{I} = (\delta_{ij})_{n\times n}$. Solving eq III.9 (by numerical methods) yields both the eigenvalues λ_j and the eigenvectors $\mathbf{v}_j$ in eq III.7. The scalar coefficients follow from the initial boundaries. Hence, from eq III.8 we find, for $t = 0$, $\mathbf{p}(0) = \mathbf{Q}(0)\mathbf{c}$ and $\mathbf{Q}(0) = [v_{ij}]_{n\times n} = \mathbf{V}$ (transform matrix). As a consequence we have $\mathbf{Q}^{-1}(0)\mathbf{p}(0) = \mathbf{c}$ with $\mathbf{Q}^{-1}(0) = [v_{ij}^{-1}]_{n\times n} = \mathbf{V}^{-1}$ containing the inverse elements. Equation III.8 can be written therefore

$$\mathbf{p}(t) = \mathbf{Q}(t)\mathbf{Q}^{-1}(0)\mathbf{p}(0) \tag{III.10}$$

After some algebra the evolution of the ith site for arbitrary initial conditions is given by

$$p_i(t) = \sum_{j=1}^{n}[v_{ij}\sum_{l=1}^{n}p_l(0)v_{jl}^{-1}]e^{\lambda_j t} \qquad i = 1, ..., n \quad \text{(III.11)}$$

The quantities $p_l(0)$ in eq III.9 are the initial site probability elements of the excitation vector $\mathbf{p}(0)$. In the case of pure positional disorder, each of the donor sites (n_D) has the same probability for direct excitation, whereas traps *per definitionem* are not subject to optical transitions. Thus the components of $\mathbf{p}(0)$ read

$$p_l(0) = \begin{cases} \frac{1}{n_D} & l = 1, ..., n_D \\ 0 & l = n_D + 1, ..., n \end{cases} \quad \text{(III.12)}$$

Using the boundaries in eq III.12 eq III.11 takes the form

$$p_i(t) = \frac{1}{n_D}\sum_{j=1}^{n}[v_{ij}\sum_{l=1}^{n_D}v_{jl}^{-1}]e^{\lambda_j t} \quad \text{(III.13)}$$

and after summation over all donors

$$p_D(t) = \sum_{j=1}^{n}\left[\frac{1}{n_D}\sum_{i=1}^{n_D}v_{ij}\sum_{l=1}^{n_D}v_{jl}^{-1}\right]e^{\lambda_j t} \quad \text{(III.14)}$$

The donor survival function $p_D(t)$ for a particular configuration is, therefore, a finite exponential series

$$p_D(t) = \sum_{j=1}^{n}\mathcal{A}_j^D e^{\lambda_j t} \qquad \mathcal{A}_j^D \doteq \frac{1}{n_D}\sum_{i=1}^{n_D}v_{ij}\sum_{l=1}^{n_D}v_{jl}^{-1} \quad \text{(III.15)}$$

which after averaging over N configurations leads to

$$\langle p_D(t)\rangle = \sum_{s=1}^{N}\sum_{j=1}^{n}\frac{1}{N}\mathcal{A}_{j,s}^D e^{-\lambda_{j,s} t} = \mathbf{L}\langle\Phi_D(\omega)\rangle \quad \text{(III.16)}$$

(index s denoting a particular configuration) which is again a finite superposition of exponentials. A similar expression can be derived for the configurative average of the trap survival probability. For N sufficiently large eq III.16 is the approximate result to the exact statistical-mechanical average ($N \to \infty$). The sum in eq III.16 can then be replaced by the integral so that in the continuum representation the donor survival function $\langle p_D(t)\rangle$ is related to the donor eigenvalue spectrum $\langle\Phi_D(\omega)\rangle$ via the Laplace transform $\mathbf{L}$ (eq III.16). A more rigorous treatment that takes into account the exact limit cases has been given in a previous publication.[12]

In the numerical calculation the quasi-continuous eigenvalues spectrum $\langle\Phi_D(\omega)\rangle$ (eq III.16) is approximated by accumulating the amplitudes $\mathcal{A}_{j,s}^D$ in m discrete channels on a (logarithmic) frequency scale, $\langle\Phi_D(\omega_i)\rangle$. The donor survival function is then, in terms of an m-fold discretization

$$\langle p_D(t)\rangle = \sum_{i=1}^{m}\langle\Phi_D(\omega_i)\rangle e^{-\omega_i t} \quad \text{(III.17)}$$

Thus, the basic steps in this simulation are as follows: (i) the MC generation of a distinct chain, (ii) assignment of sites, the reading-in of the site coordinates r_i for calculating the transition rates (eq III.4) and thus the elements of the transition matrix $\mathbf{W}$ (eq III.2), (iii) the calculation of amplitudes $\mathcal{A}_{j,s}$ and eigenvalues λ_j (eqs III.9, III.15), (iv) the construction of the configurational average of the eigenvalues spectrum, $\langle\Phi(\omega_i)\rangle$, by repeating steps i–iii for a statistically relevant number of chains ($N = 10^4$), and (v) the construction of the survival function $\langle p(t)\rangle$ via Laplace transform (eqs III.16, III.17).

IV. Results

Reduced variables ω_i and t have been used in the forthcoming representation, so ω_i is normalized to the nearest-neighbor donor–trap (D–T) transfer rate η_0^{DT} and t_r to its inverse, $1/\eta_0^{DT}$, respectively. Furthermore, it proves useful to define a coupling strength r as the ratio of nearest-neighbor transition rates for D–D transfer and irreversible trapping (DT), $r = \eta_0^{DD}/\eta_0^{DT}$. What we wish to demonstrate in this work is the effect of trap location and chain dimension on the dynamics of irreversible excitation trapping, i.e. the relaxation functions $\langle\Phi(\omega_i)\rangle$ and $\langle p(t)\rangle$. Related problems concerning trap position in random chains have been discussed on the basis of a different approach by Webber's group, very recently.[20] Here chain configurations with a single trap per chain have been generated and the trap has been placed (i) in a randomly distributed fashion along the chain and (ii) at the end of the chain. A chain length $L = 50$ (49 donors, 1 trap) has been used in preliminary calculations, and for 2-D and 3-D chains, the number of polymer realizations has been chosen to be $N = 10^4$ to obtain relevant averages.

To begin, we focus on the random trap system and examine the effect of chain dimensionality on the pattern of D–T transitions, first, in the absence of D–D multistep interactions ($r = 0$). In this case, the system is decoupled and the eigenvalues of $\mathbf{W}$ are the diagonal elements of $\mathbf{W}$: $\omega_i = \nu_i \doteq \sum_{l=n_D+1}^{n}\gamma_{il}^{DT}$. The $\Phi_D(\nu_i)$ pattern at the top of Figure 1a shows the linear chain with a characteristic single-peak progression that corresponds to the transitions in the 1-D chain, i.e. nearest-neighbor ($\log \nu_i/\eta_0^{DT} = 0$), next-to-nearest-neighbor, and nonnearest neighbor. The curved intensity profile of amplitudes is a direct consequence of the DT distance distribution for a linear chain of lengths L in the case of a single trap $S_i \propto L - i$ ($i = 1, ..., L - 1$)[21] and its functional form in the ν space. The pattern in the middle represents the configuration-averaged spectrum $\langle\Phi_D(\nu_i)\rangle$ for the 2-D chain. Comparison with the upper spectrum exhibits the typical feature of quadratic lattice chains, i.e. the occurrence of nonnearest, nonbond transitions. These contacts shorten the distances between D and T and hence enforce the trapping process by decreasing the residence time of donor excitation. The overall effect of this competition is, therefore, to decrease the contribution of amplitudes in the utmost long-distance, low-frequency regime, and this tendency is, naturally, increased in the 3-D chain (see, $\langle\Phi(\nu_i)\rangle$ at the bottom). The reduction of D–T transfer pathways with increasing nonbond contacts, naturally, shortens the donor relaxation scale, as can be seen from the time-domain analogs $\langle p_D(t)\rangle$ (eq III.17) in Figure 1b, (from top to the bottom: 1-D, 2-D, 3-D).

In the following calculations the unperturbed spectrum $\langle\Phi_D(\nu_i)\rangle$ of single-step D–T transitions (Figure 1a) is chosen as a reference pattern for illustrating the perturbation of multistep donor–donor (D–D) transitions ($r > 0$).

In Figure 2a the interfering effect of very weak D–D coupling ($r = 10^{-3}$) is shown for the linear chain (top), the 2-D chain (middle), and the 3-D chain (bottom). The minimal D–D interaction stimulates, naturally, the very slow D–T transitions between (long-distance) nonnearest neighbors, both via bond and nonbond contacts (2-D, 3-D), thus annihilating the characteristic single peak progression in this frequency regime. In comparison with the unperturbed case ($r = 0$, Figure 1a) the eigenvalues spectrum

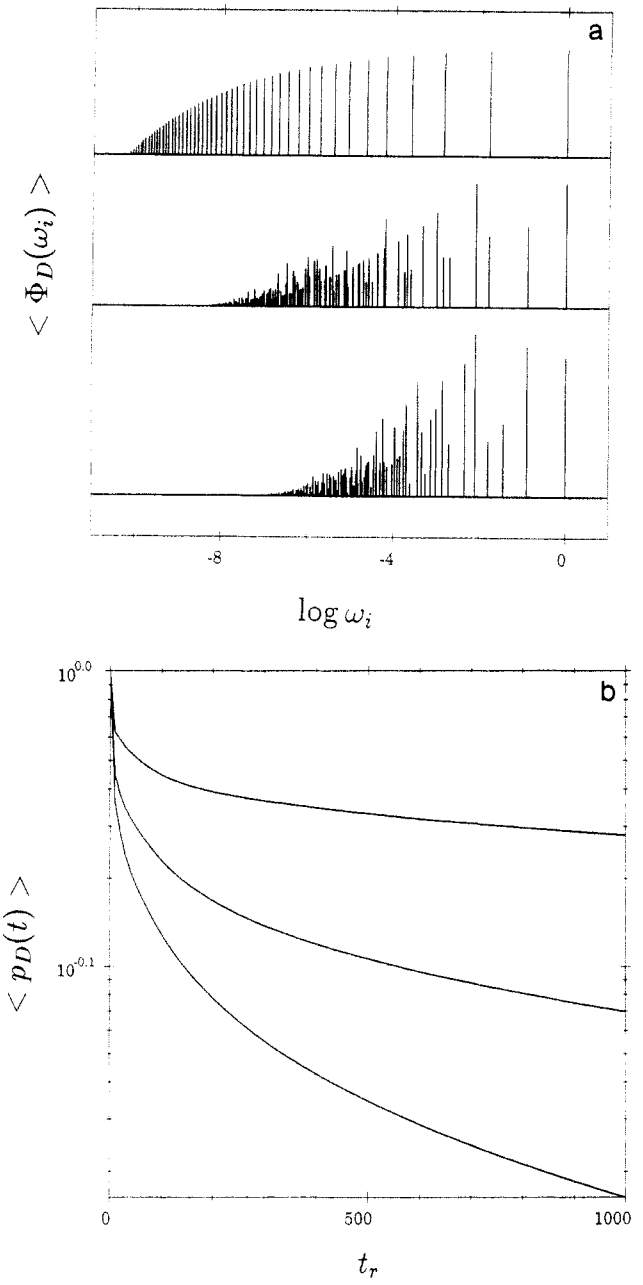

Figure 1. (a) Effect of dimensionality on the distribution of single-step transitions ($r = 0, \omega_i = \nu_i$) for lattice chains with random trap placement (49 donors, 1 trap): (from top to the bottom) 1-D, 2-D, 3-D. Note that the patterns for 2-D and 3-D topologies represent ensemble averages of random chains. $\omega_i = \nu_i$ are reduced in units of η_0^{DT}. (b) Time-domain analogs obtained from Figure 1a by Laplace transform (eq III.17). The decays $\langle p_D(t) \rangle$ from top to bottom correspond to 1-D, 2-D, and 3-D, respectively. The time scale is in units of $1/\eta_0^{DT}$; see text for details.

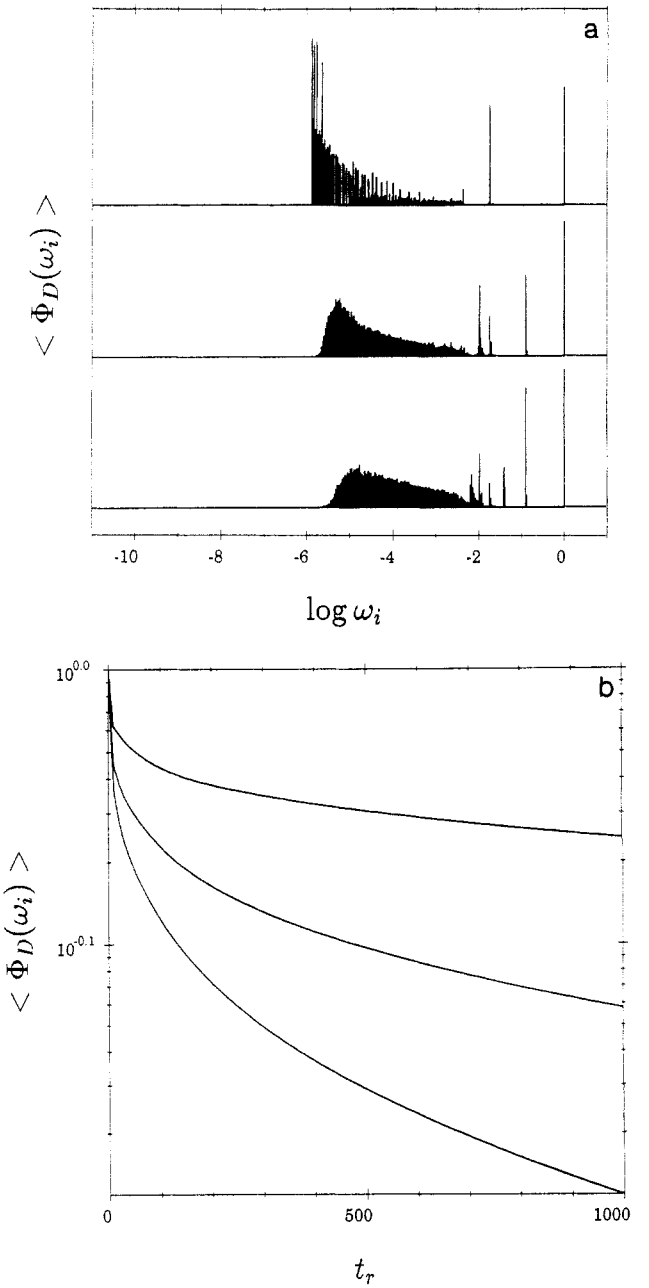

Figure 2. (a) Influence of minimal D–D coupling ($r = 10^{-3}$, in units of η_0^{DT}) in 1-D, 2-D, and 3-D chains (top to bottom) with random trap location (49 donors, 1 trap). Note the predominant hopping modes in the intermediate-to-low frequency regime (ω_i reduced in units of $1/\eta_0^{DT}$). See the unperturbed case in Figure 1a for comparison. (b) Donor survival probabilities $\langle p_D(t) \rangle$ analogous to the frequency-domain solutions $\langle \Phi_D(\omega_i) \rangle$ in Figure 2a. Fast to slowest decays correspond to 3-D, 2-D, and 1-D, respectively.

$\langle \Phi_D(\omega_i) \rangle$ of Figure 2b exhibits (i) a cutoff in the utmost low-frequency regime and (ii) a quasi-continuum in the intermediate ω_i space for 2-D and 3-D chains. Note that the very weak D–D coupling chosen here leaves nearest-neighbor, next-to-nearest-neighbor, and (short-distance) nonbond transitions intact, to a good approach. This situation is equivalently represented in the time domain (Figure 2b): slowest to fast donor survival functions $\langle p_D(t) \rangle$ correspond to 1-D, 2-D, and 3-D respectively.

Increasing the D–D coupling initiates the competition with the high-frequency single-step D–T events, so even for moderate coupling $r = 1$ the net result is a complete vanishing of these transitions (Figure 3a). For 2-D and 3-D chain topologies, $\langle \Phi_D(\omega_i) \rangle$ becomes quasi-continuous over the entire frequency scale, with the central mean $\langle \omega \rangle$ shifting to higher values and thus, accelerating the donor decay (Figure 3b, see caption for details). When going to larger coupling strengths ($r = 10, 100$) the $\langle \Phi_D(\omega_i) \rangle$ patterns generally undergo a distinct spectral narrowing and this tendency in the ω domain is equivalent to a gradual exponentialization of the time-domain solutions.[12]

In Figure 4a we have computed the extreme situation of multistep dynamics with D–D coupling set at $r = 10^{10}$ (from top to bottom: 1-D, 2-D, and 3-D). Here the donor excitation has reached the rapid transfer limit where the dynamics is mainly controlled by the averaged frequency of D–T transfer, $\overline{\nu^{DT}}$.[12] The central issue of these calculations is (i) the finite width of $\langle \Phi_D(\omega_i) \rangle$ caused by averaging

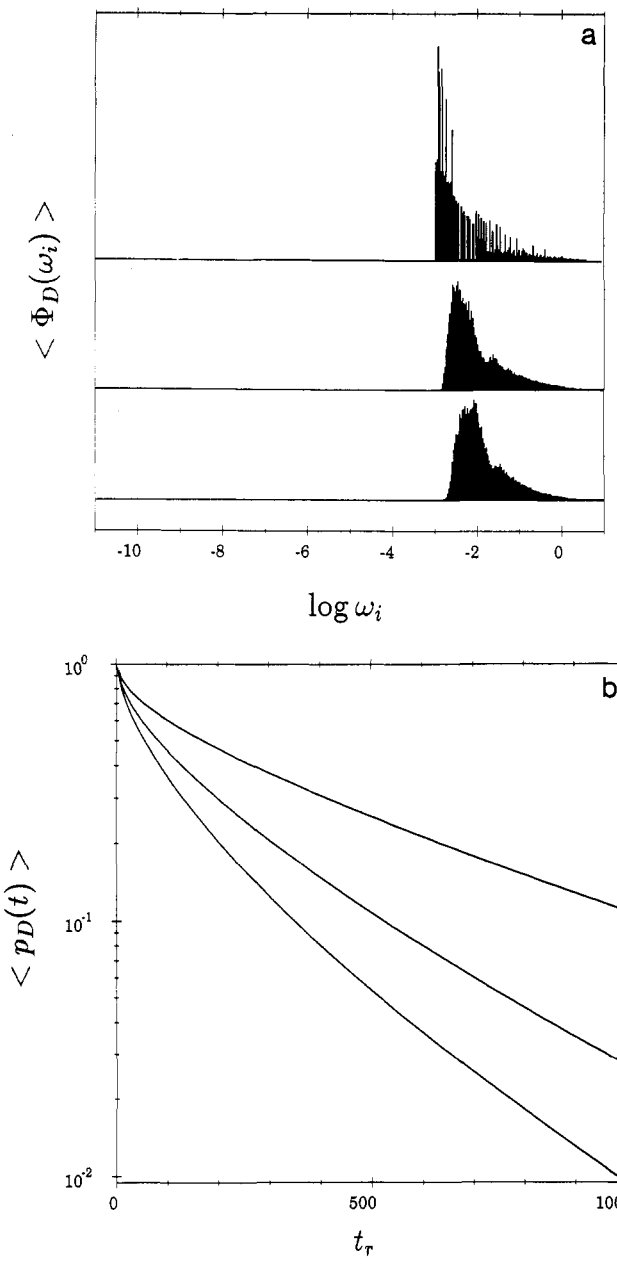

Figure 3. (a) Increased D–D coupling (r = 1), gradual spectral narrowing, and tendency toward quasi-continuous amplitudes—due to D–D multistep modulation.[12] Same donor and trap ensemble as above. From top to bottom: 1-D, 2-D, and 3-D, respectively. (b) Time-domain solutions equivalent to mode-frequency spectra in Figure 3a. From top to bottom the $\langle p_D(t) \rangle$ profiles correspond to 1-D, 2-D, and 3-D, respectively.

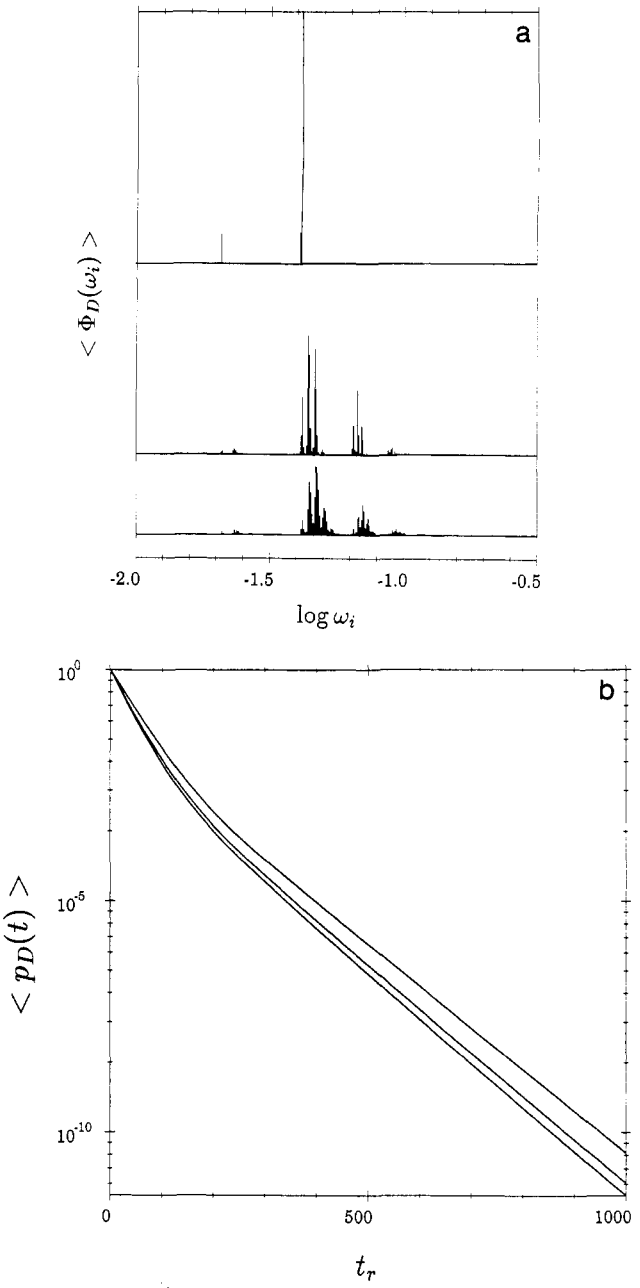

Figure 4. (a) $\langle \Phi_D(\omega_i) \rangle$ spectra in the rapid transfer limit, $r \to \infty$ ($r = 10^{10}$ in these computations). Upper to lowest pattern refer to 1-D, 2-D, and 3-D, respectively. The spectra have finite widths and show a substructure that reflects the lattice chain model.[12] (b) Time-domain analogs, slowest to fast $\langle p_D(t) \rangle$ decays correspond to 1-D, 2-D, and 3-D.

finite single chains and (ii) the significant fine structure of $\langle \Phi_D(\omega_i) \rangle$ which—because of the low trap density (one trap per chain)—directly reflects the number of contacts Z in our chain model: Z = 1, 2 for 1-D [top, frequencies at log(1/49) and log(2/49)]; Z = 1–4 for 2-D (middle) corresponding to the lower-bound frequencies at log(1/49), log(2/49), log(3/49), log(4/49); and Z = 1–6 for 3-D (bottom) with additional frequencies located at log(5/49) and log(6/49), respectively. Details pertaining to the analytical treatment of this limit are given in our recent work.[12]

Next we will concentrate on the question of how trap position (end-tagged vs random assignment) will affect the shape of the eigenvalues spectrum for a 1-D chain (49 donors, 1 trap). The parameter that has been varied is again the D–D coupling strength (r = 0, 10^{-3}, and 1, respectively).

In Figure 5a, first, the uncoupled limit r = 0 has been calculated, i.e. the single step D–T frequency distribution for both chains, $\langle \Phi_D(\nu_i) \rangle$. While the upper pattern represents the discrete rectangular distribution $\langle \Phi_D(\nu_i) \rangle$ characteristic for the linear chain with a terminal trap (a single conformation, only), the curved spectrum at the bottom displays the linear chain with random trap distribution and represents an ensemble average [see also Figure 1a, top]. Figure 5b demonstrates how the uncoupled spectra $\langle \Phi(\nu_i) \rangle$ in Figure 5a are affected by very weak D–D coupling ($r = 10^{-3}$). Again, the typical cutoff for both 1-D chains is found (see also the spectrum in Figure 2a, top), the lowest frequency ω_i carrying the maximum amplitude value for the end-tagged polymer, no matter what the strength of coupling is [see Figure 6a below]. The positions of high-frequency transitions remain constant for both types of chains; i.e. nearest- and next-to-nearest-neighbor D–T single-step jumps are nearly

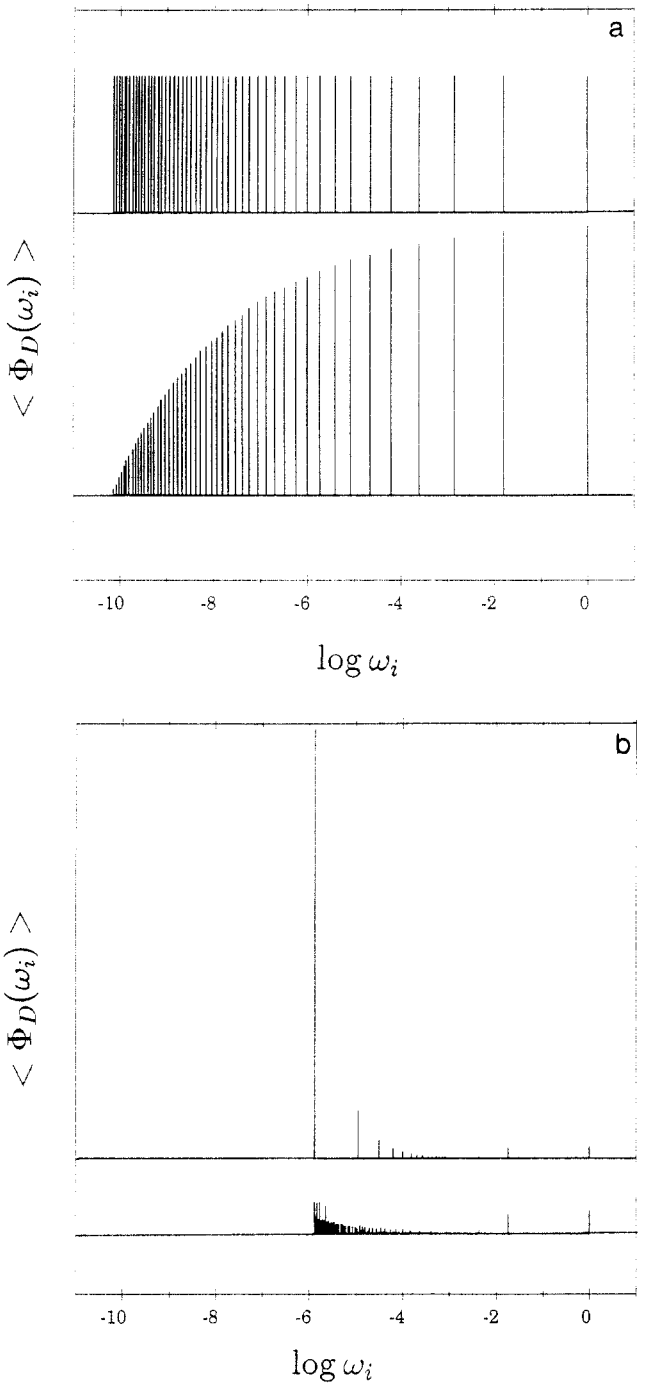

Figure 5. (a) Distribution of single-step transition frequencies ($r = 0$, $\omega_i = \nu_i$) in a 1-D chain: random (upper spectrum) vs terminal trap location (lower spectrum); 49 donors, 1 trap. Random trap placement produces disruptive chains with different statistical weights; see the text. (b) Minimal perturbation by weak D–D coupling ($r = 10^{-3}$): (upper spectrum) end-tagged 1-D chain; (lower pattern) 1-D chain with random trap distribution. Weak perturbation leaves intact nearest-neighbor and next-to-nearest-neighbor D–T transitions; different density of states for terminal and random trap assignment.

unperturbed, whereas the amplitudes of transitions in the intermediate-to-low-frequency regime correspond to frequencies of hopping modes. The spectrum $\langle \Phi_D(\omega_i) \rangle$ is discrete in the end-tagged chain (top) but shows a high density of states in the random trap polymer (bottom). In the latter case, the pattern can be understood as a superposition of eigenvalues spectra of subchains that have lower donor dimensions, the distribution of disruptive chains arising from the random placement of traps along the chain.

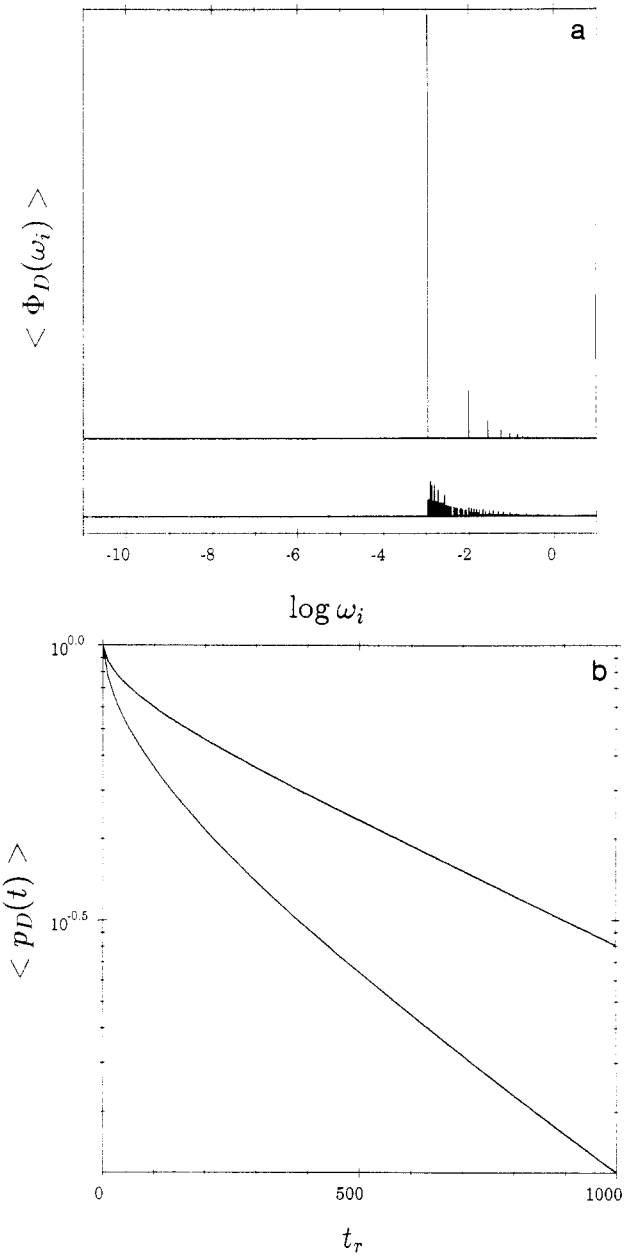

Figure 6. (a) Typical blue shift of mode spectra $\langle \Phi_D(\omega_i) \rangle$ paralleled by the annihilation of nearest-neighbor transitions, when further increasing the coupling strength ($r = 1$): See Figure 5a,b for comparison. (b) Laplace transform analogs $\langle p_D(t) \rangle$: (upper curve) terminal trap; (lower profile) random trap 1-D chain.

With further increasing the D–D coupling strength ($r = 1$), we find the terminal, intense amplitude typical for the end-tagged 1-D chain shifted to higher frequency ($\log \omega = -3$) followed by a series of high-frequency transitions that overwhelm the positions of the high-frequency, single-step D–T events (upper pattern). The same tendency is observed for the 1-D chain with random trap distribution, the high density of amplitudes being caused by the manifold of trap positions along the chain which produces a large superposition of lower dimensional eigenvalues spectra (lower spectrum, averaged). The time-domain solutions equivalent to the $\langle \Phi_D(\omega_i) \rangle$ graphs are given in Figure 6b. A statistical distribution of traps along the chain creates, on the average, shorter transport pathways, so excitation trapping relaxes faster in the 1-D chain with random trap locations (lower curve). However, the differences of the decays are marginal (see extended intensity scale in Figure 6b). For the lower coupling

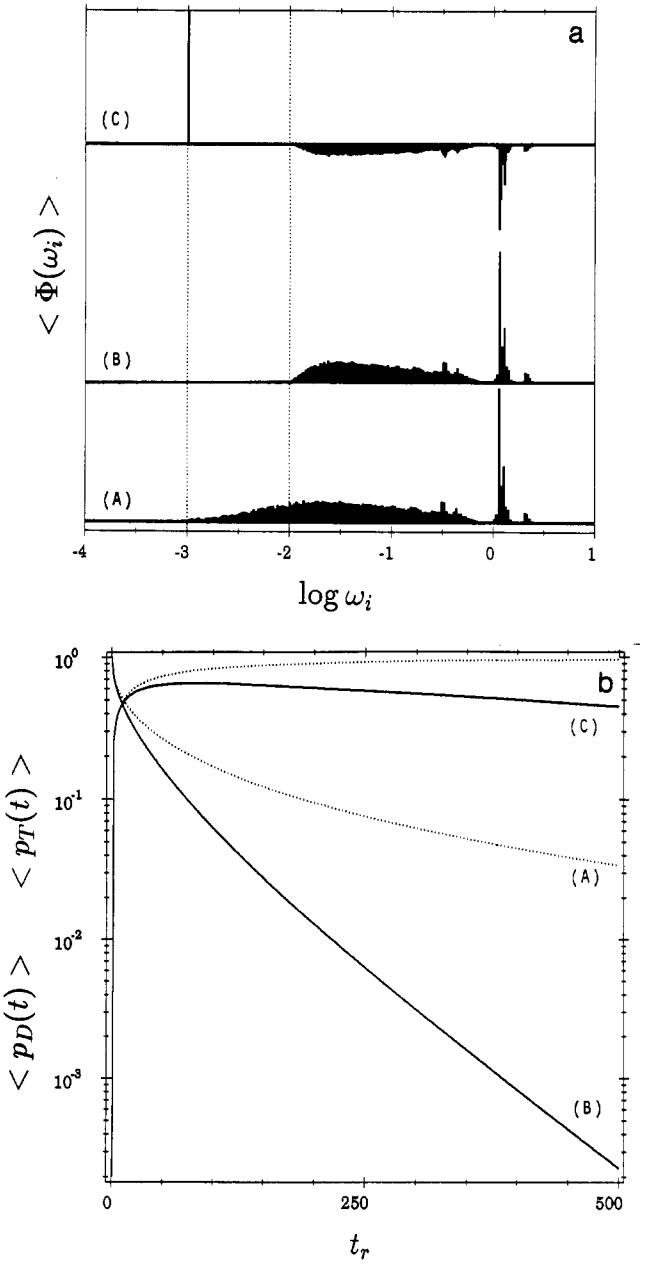

Figure 7. (a) Effect of fluorescence cutoffs $k_D = 10^{-2}$ and $k_T = 10^{-3}$ (in units of η_0^{DT}) in the irreversible trapping limit: (A) in the absence of radiative deactivation; (B) $\langle \Phi_D(\omega_i) \rangle$ in presence of donor fluorescence; (C) the eigenvalues spectrum of the trap, $\langle \Phi_T(\omega_i) \rangle$, in presence of trap fluorescence (negative amplitudes due to migrative population). The signal at $\log \omega = -3$ represents the asymptotic decay behavior controlled by the trap fluorescence process. 3-D SSAW chains, 90 donors, 10 traps. (b) Analogous time-domain solutions: (A) survival function $\langle p_D(t) \rangle$ in the absence of deactivation; (B) (δ-pulse) donor fluorescence response; (C) evolution of trap fluorescence.

strengths in Figure 5a,b similar time-domain analogs can be assembled that can be hardly distinguished on usual intensity scales. From the experimental point of view, one would expect, therefore, that the two polymer topologies are barely resolvable from high-precision fluorescence raw data.

In Figure 7 the effect of *fluorescence deactivation* on the evolution of hopping processes in a polymer is examined, which is just the microscopic scenario concealed in a transient fluorescence trapping experiment.[5] In these experiments the trap density is $\rho_T = 0.1$ and the placement of the trap across the chain is random. D–D coupling has been chosen to be $r = 0.1$, and the radiative dynamics has been modeled for both the donor and the trap sites. In the following run the reciprocal fluorescence lifetimes have been chosen to be $1/\tau_D = k_D = 10^{-2}$ and $1/\tau_T = k_T = 10^{-3}$, respectively (both normalized to η_0^{DT}). Situation A displays the donor eigenvalues spectrum $\langle \Phi_D(\omega_i) \rangle$ in the absence of fluorescence; the origin of these transition modes has been extensively discussed in our previous paper.[12] Situation B displays the donor eigenvalues spectrum $\langle \Phi_D(\omega_i) \rangle$ under the influence of fluorescence with the typical cutoff for frequencies $\log \omega_i = 2$—due to the radiative damping ($k_D = 10^{-2}$, vertical dotted line). The pattern in (C) refers to the eigenvalues spectrum of the trap $\langle \Phi_T(\omega_i) \rangle$ with formally *negative* amplitudes that illustrate the characteristic migrative population of the trap, equivalent to the nonexponential rise term in the time-domain profile [see Figure 7b (C)]. The positive amplitude positioned at $\log \omega_i = -3$ reflects the fluorescence decay of the trap ($k_T = 10^{-3}$) which exactly equals the sum of the negative amplitudes (the size of the positive amplitude not appropriately scaled in this representation). The time-domain analogs are displayed in Figure 7b. (B) and (C) are the theoretical δ-pulse solutions of donor and trap fluorescence, whereas the dotted profiles represent the survival probabilities for donor (A) and trap, respectively, in the absence of radiation. For the kinetic parameters chosen in our example, a radiative channel thus increases the decay by eliminating the low-frequency tail of $\langle \Phi(\omega_i) \rangle$. The choice of the lifetimes ($\tau_D \ll \tau_T$) also implies that the intermediate-to-long-time decay of the trap fluorescence is monoexponential. Note that this condition does not necessarily hold and the converse is true for $\tau_D \gg \tau_T$. In this case the migrative fluorescence decay of the trap is controlled by a bundle of (positive) low-frequency amplitudes which produce a nonexponential decay pattern. An example illustrating the situation $\tau_D \gg \tau_T$ will be given for a reversible system (see Figure 9 below).

IV.1. Reversible Migrative Trapping. In the case of reversible donor–trap interaction ($\gamma_{ij}^{TD} \neq 0$) the excitation matrix **W** is nonsymmetric. The evolutions of the donor and trap ensemble are therefore coupled which requires the n-dimensional eigenvalue problem to be solved (in lieu of the reduced n_D dimensionality in the irreversible limit; cf. preceding subsection).

In Figure 8 we show how detrapping (trap–donor backtransfer) affects the donor fluorescence decay, while keeping the remaining parameters fixed. In Figure 8a from bottom to top, the strength of trap dissociation $q = \eta_0^{TD}/\eta_0^{DT}$ has been varied for T→D coupling parameters $q = 0$ (A), 0.01 (B), 0.1 (C), and 1 (D) (in units of η_0^{DT}), respectively. Our doorway situation (A) is the donor eigenvalues spectrum for the irreversible case ($q = 0$) with $\rho_T = 0.1$, $r = 0.1$ and the same cutoff parameters $k_D = 10^{-2}$ and $k_T = 10^{-3}$ (in units of η_0^{DT}) as used in Figure 7a (situation B). Evidently, the effect of a weak reversible constraint, e.g. $q = 0.001$, is to induce a small perturbation to the overall migrational sampling process, only (B). The weak dissociation is clearly manifested by the appearance of a bundle of low-intensity amplitudes centered at $\log \omega_i = -2.8$, characteristically shifted from the irreversible limit (dotted vertical lines at positions $\log k_D = -2$ and $\log k_T = -3$). Quite obviously, the donor ensemble "feels" the trap only in the ultimate low-frequency regime of its mode spectrum, but is practically not affected in the moderate-to-high mode frequency regime. When the T→D coupling is increased (C), the group of low-frequency, low-intensity amplitudes grows at the expense of the amplitudes at higher frequencies ($\log \omega_i > 0$), with a central mean that shifts to higher frequencies ($\log \omega = -2.3$). In the case of strong detrapping (situation D) the ensemble of modes

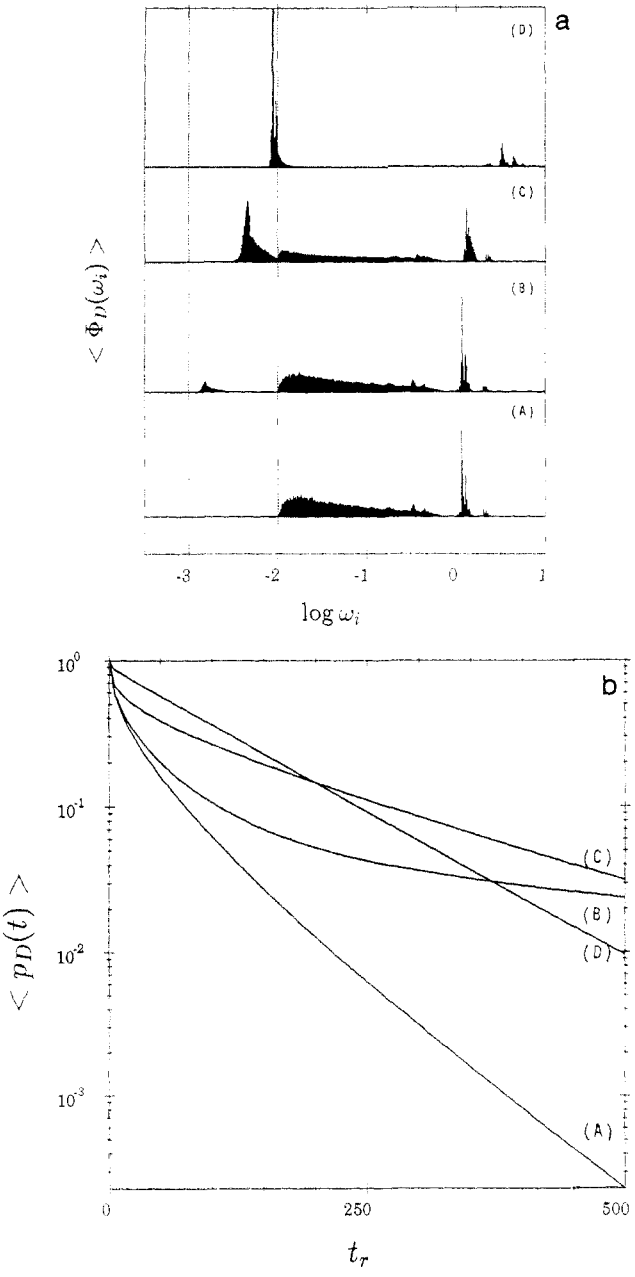

Figure 8. (a) Effect of detrapping $q = \eta_0^{TD}/\eta_0^{DT}$ on $\langle \Phi_D(\omega_i) \rangle$ in the presence of radiation (N = 5000, 3-D chain with 90 donors and 10 sites; moderate coupling r = 0.1). The curves from bottom to top have the following (reduced) detrapping parameters, q = 0 (A), 0, 01 (B), 0.1 (C), and 1 (D), respectively. Dotted lines show the frequency locations of radiative cutoffs k_D and k_T. (b) Laplace transform solutions; the profiles represent the donor fluorescence responses as a function of detrapping. Again, curves A–D correspond to q = 0, 0.01, 0.1, and 1, respectively.

ends up in a complete flowing-off of amplitudes in the intermediate frequency regime which yields an approximate bimodal pattern consisting of narrowly spaced modes with, in part, high-intensive amplitudes around log ω = −2.1 and a collection of low-intensity signals located in the high-frequency regime around log ω = 0.5.

Figure 8b shows the corresponding Laplace transforms. The curves represent the δ-pulse donor fluorescence response of the system and illustrate how the degree of reversibility affects the entire (nonexponential) profile [from bottom to top: q = 0 (A), 0.001 (B), 0.1 (C), and 1 (D), respectively]. Increasing the strength of back-transfer leads to an enhanced probability of repopulating a donor site, so this revisiting shows up in a systematic slowing down of the donor fluorescence. The fluorescence process, however, causes the various decays to intersect at different times, thus the systematic trend of deceleration for the fluorescence curves as a function of growing detrapping is only relevant in front of the (first) crossing point, the length of this time regime, naturally, being dependent on the choice of the radiative rate constant k_D. Generally, the enhancement of reverse coupling tends to exponentialize the donor decay (D), but note that neither the low-intensity short-time behavior nor the intermediate relaxation scale in Figure 8b is, in fact, single-exponential, due to the finite width of the eigenvalues spectrum underlying the decay (situation D, Figure 8b).

So far the fluorescence lifetime of the trap ($1/k_T$) has been chosen 1 order of magnitude larger than the donor lifetime ($1/k_D$). In aromatic chromophores for red shifted traps this condition does not necessarily hold. In Figure 9 the effect of reverse constraints is demonstrated for radiative cutoffs $k_D = 10^{-3}$ and $k_T = 10^{-1}$ (normalized to η_0^{DT}), thus $\tau_D/\tau_T = 10^2$. The same trap density has been chosen (ρ_T = 0.1), and D–D coupling in the intermediate regime (r = 1) has been assumed (N = 5000 configurations). Again, the detrapping ratio q varies (from bottom to top: q = 0, 0.01, 0.1, and 1, respectively). $\langle \Phi_D(\omega_i) \rangle$ at the bottom represents the irreversible case practically unaffected by the (extreme) positions of cutoffs k_D and k_T. On the one hand, k_D (dotted vertical line at log ω_i = −3) is far away from the range of frequency modes $\{\Phi_D(\omega_i)\}$, so the fluorescence decay is too slow to "feel" the hopping dynamics. On the other hand, k_T (dotted vertical line at log ω_i = −1) coincides with $\langle \Phi_D(\omega_i) \rangle$, but this has no effect—due to the strict irreversibility of the situation (q = 0). In the case of minimal perturbation (reversible D–T interaction), the typical section of $\langle \Phi_D(\omega_i) \rangle$ becomes apparent, immediately. The node centered at log k_T = −1 leads to a phenomenologically bimodal distribution, its components being separated more and more with increasing detrapping and, gradually, ending up in a (low-intensity) high-frequency and an intense low-frequency branch. The corresponding time-domain solutions are displayed in Figure 10b. Generally, the spectra narrow and the decays tend to exponentialize for $q \rightarrow \infty$, but note that the Birks limit[22] can never be reached, due to the finite size of the polymer.

V. Summary and Concluding Remarks

What we wished to demonstrate in this paper is that computer simulation is a powerful tool for describing microscopic aspects of incoherent excitation transfer in simple chain models. The problems addressed here have been concerned with (i) single-step D–T transfer and (ii) migrational (D–D assisted) excitation trapping, both in the low trap (Figures 1–7) and in the moderate trap density regime (Figures 8–10). The study has focused on the calculation of optical dynamics for various D–D coupling strengths r, with special emphasis placed on the influence of trap position and chain dimension, and on the effects of radiative cutoff and reverse D–T transitions. Isoenergetic donor sites have been chosen and all interactions (no cutoff) have been assumed to be dipolar, in nature (cf. below).

The calculation of frequency- and time-domain solutions for both donor and trap relaxation has been performed by a Monte-Carlo standard chain generation combined with a master equation solution routine. The quantity computed by diagonalization and effective averaging over typically $N = 10^4$ chain realizations has been (i) the eigenvalues spectrum for the donor $\langle \Phi_D(\omega_i) \rangle$ and the trap

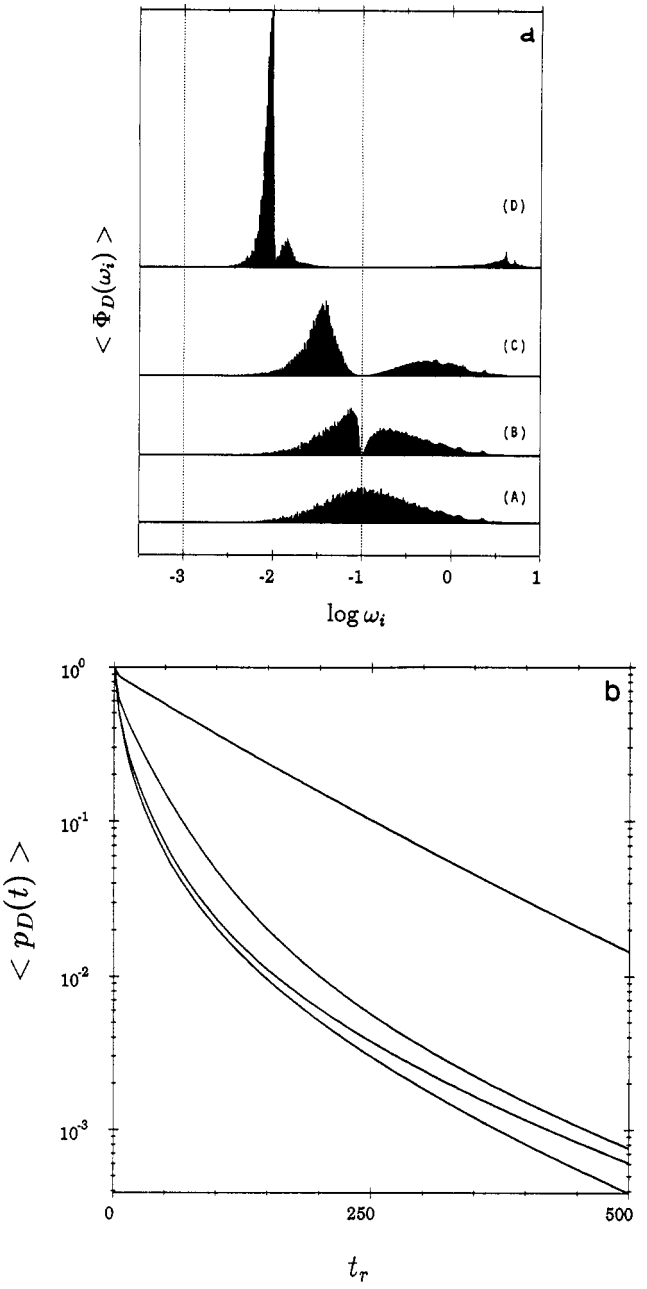

Figure 9. (a) Effect of radiative cutoffs $k_D = 10^{-3}$ and $k_T = 10^{-1}$ (in units of η_0^{DT} on the eigenvalues spectrum $\langle \Phi_D(\omega_i) \rangle$ for various detrapping strengths $q = \eta_0^{TD}/\eta_0^{DT}$: [from bottom (A) to top (D)] $g = 0, 0.01, 0.1$, and 1, respectively. The D–D coupling has been set at $r = 1$ in these computations. The patterns of $\langle \Phi_D(\omega_i) \rangle$ differ quite markedly from those in Figure 8a which is due to the difference cutoff ratio $k_D/k_T = 10^{-2}$ chosen in this calculation. (b) Equivalent time-domain solutions: (from bottom to top) $q = 0$, 0.01, 0.1, and 1, respectively.

$\langle \Phi_T(\omega_i) \rangle$ and (ii) [via Laplace transform (eq III.16)] the survival probability $\langle p_D(t) \rangle$ and $\langle p_T(t) \rangle$ for the donor and trap, respectively.

It has been our objective to show that $\langle \Phi(\omega_i) \rangle$ is an effective tool for probing different photophysical situations of migrative trapping in a polymer and a sensitive terminal for mapping out the characteristic changes of polymer-inherent transitions that can be affected by varying the parameters of transport and trapping on a microscopic molecular level. In particular, when the (averaged) amplitudes $\langle \Phi(\omega_i) \rangle$ were plotted over $\log(\omega_i)$, the spectra proved extremely useful in delineating the complex interplay between serial D–D (multistep) and parallel D–T (single step) transitions among nearest-, next-to-nearest-, and nonnearest-neighbor contacts on the lattice. Situations that have been simulated by this technique are the rapid D–D transfer limit (Figure 4), the weak-to-intermediate D–D coupling regime (Figures 2, 3, 5b, and 6), the unperturbed case of vanishing D–D interaction (Figures 1 and 5a), the effect of a radiative cutoff (fluorescence deactivation) on the shape of $\langle \Phi(\omega_i) \rangle$ [Figure 7a for both the donor (situation B) and the trap sites (situation C)] and the role of D–T back-transfer (Figures 8–10) in the weak-to-intermediate D–D coupling regime.

In the absence of D–D migration (Figures 1a and 5a) the direct donor–trap transitions span a broad spectrum of transfer rates with a pronounced substructure that allows the assignment of nearest-neighbor, next-to-nearest-neighbor, and nonnearest-neighbor contacts among bonded and nonbonded sites. The computation clearly demonstrates how increasing D–D intersite perturbation (Figures 2a, 3a, 5b, and 6a) affects the zeroth-order eigenvalues spectrum of the decoupled problem. In the intermediate D–D coupling regime with η_0^{DD} and η_0^{DT} approaching a comparable order of magnitude $\langle \Phi_D(\omega_i) \rangle$ is systematically narrowed as a result of the modulating power of transport and the structure of the spectrum complicates more and more, due to the complex spatio-temporal evolution of high-dimensional, migrating excitations and the multitude of polymer chain configurations used in the averaging procedure. Spectra in Figure 4a correspond to strong D–D coupling and exemplify how rapid migrative transitions between donor sites will affect the slower event of D–T trapping. This situation approaches the rapid transfer limit very well where the intersite D–D transfer is so rapid that the donor ensemble is essentially equilibrated on the time scale of D–T trapping. This tendency toward rapid equilibrium is paralleled by a further narrowing of $\langle \Phi_D(\omega_i) \rangle$, the extent of migrational narrowing depending on the choice of the r parameter and the number of chain realizations in the configurational space. Note that the width of $\langle \Phi_D(\omega_i) \rangle$ never ends up in a δ-function, i.e. a single exponential time domain response when going to the limit $r \to \infty$, due to the finite size of our chain model. Furthermore, the spectra exhibit a pronounced infrastructure which directly maps out the number of contacts of the underlying lattice chain. Both regimes, i.e. the $r = 0$ and the $r = \infty$ limit are kinetic fingerprints of the conformational disorder of the underlying polymer lattice model; thus both limits allow structural parameters to be extracted. In the intermediate D–D coupling regime, however, the effect of excitation transfer is to modulate and to smear out the probability amplitudes. So the disappointing conclusion is that less structural information can be drawn in the presence of migrational sampling.[12]

Comparison of Figures 1 (and 2 and 3) and 5a and 5b and 6a finally shows how chain dimension and trap position affect $\langle \Phi(\omega_i) \rangle$ and, thus, the relaxation properties of a donor excitation. Such simulations are intended to improve our understanding in trapping experiments, in particular, as the pathways of transfer are anisotropic and the location of traps are, generally, unknown in real polymers that makes a disentangling of this quantities hardly tractable and the interpretation of such data, in any case, controversial.

In Figures 1–6 the frequency- and time-domain solutions have been calculated in the absence of fluorescence. In Figure 7 the relaxation patterns include a radiative rate. The objective of this computation has been to demonstrate the cutoff effect executed by a radiative deactivation on the mode frequency spectrum $\langle \Phi(\omega_i) \rangle$. Under conditions where the intrinsic donor lifetime τ_D coincides with the

spectral range of $\langle\Phi(\omega_i)\rangle$, the role of the fluorescence channel is to eliminate the entire set of transition frequencies ω_i with values smaller than $1/\tau_D$, thus increasing the overall decay. In this case the fluorescence process eliminates the interesting structure of long-range nonnearest transitions. On the other hand, an inverse donor lifetime $1/\tau_D$ that is small compared to the central mean of $\langle\Phi(\omega_i)\rangle$ has no cutoff effect and, hence, can hardly "feel" the hopping events. In this scenario (not computed here), the decay is predominantly monoexponential, so no information about the time-dependent amplitudes in the $\langle\Phi(\omega_i)\rangle$ spectrum is available from a fluorescence experiment. Note that all calculations done in Figure 7 are based on the factorization concept for *irreversible* fluorescence trapping which allows the jump dynamics and the fluorescence events to be partitioned and thus to be treated independently from each other.

Another issue in this calculation has been the simulation of the migration process in the presence of *detrapping* where distributed transitions from the trap to the ensemble of donors can occur (Figures 8–10). From the physical point of view, this situation corresponds to the thermal release of a trapped excitation from a shallow trap as a result of phonon or libration induced promotion. Another mechanism of detrapping—although not operative on the premises of immobile sites considered here—is the dissociation of excimer forming sites as a result of conformational motion in a polymer.[23] Qualitatively, backtransfer leads to an enhanced probability of revisiting a donor site, thus increasing the exploration volume of an optical donor excitation. From a quantitative point of view, however, the reversibility in distributed trapping encounters severe mathematical complications which cannot be solved analytically in the time domain, even for random systems. While both the WKB[24] and a perturbation theory solution[25] represent expressions in the limit of weak coupling, convolution techniques yield formally exact solutions in the Laplace space.[26] The simulation presented here has the advantage of circumventing all these analytical difficulties, as it solves the problems as it stands.

Several conclusions may be reached from our study that may provide some general guidelines for experimentalists in analyzing their data.

(i) The effects of varying trap location and dimensionality (Figures 1–6) on the migration dynamics are illustrative in the frequency regime [$\langle\Phi(\omega_i)\rangle$], but not very pronounced in the time domain. Note that, in particular, in the case of varying dimensionality (Figures 1–3) the curves to be compared correspond to small intensity changes on very large time scales (t_r is in units of η_0^{DT}). Since the $\langle p(t)\rangle$ response multiplied with a constant exponential of the inherent fluorescence process represents the kernel of the experimental convolution integral (*vide infra*) and thus is smoothed by the integral operator and the noise statistics, we conjecture that it must be, indubitably, a difficult enterprise to find such slight differences in real data. High-precision data at a 10^5 up to 10^6 count level at the peak maximum would be required to detect the slight difference on the basis of the usual goodness-of-fit criteria. To our knowledge there exist no experimental results, so far, that might corroborate these considerations.

(ii) The frequency analog $1/\tau_D$ of the fluorescence process must sufficiently interact with the frequency modes of the hopping process in order to be a sensitive terminal for probing excitation transfer in a polymer. Thus the spectral position of $1/\tau_D$ on the frequency scale of $\langle\Phi(\omega_i)\rangle$ determines the extent of intersection, these quantities being, naturally, a function of the molecular transition dipole, the oscillator strength, and the electronic coupling matrix of the interchromophoric interaction. Short-lived chromophores with lifetimes on a picosecond time scale are expected therefore to cut off the interesting structure of $\langle\Phi(\omega_i)\rangle$ in the low-to-moderate frequency part, but they have the advantage of probing the high-frequency wing due to the sufficient fluorescence signal intensity on this time scale. On the other hand, when using the conventional long-lived nanosecond probe chromophores, a larger contribution of low frequencies from $\langle\Phi(\omega_i)\rangle$ should be available from high-precision single-photon-counting (SPT) fluorescence experiments. This optimal adjustment in the context with picosecond SPT seems to be verified in copolymers with 2-vinylnaphthalenes as the optically active component in recent fluorescence depolarization studies.[27] However, the high-frequency tail of $\langle\Phi(\omega_i)\rangle$ is, of course, not accessible by such an experiment. But we conjecture that with the femtosecond laser-band limited method of fluorescence frequency conversion optical gating[28] these high-frequency contributions of $\langle\Phi(\omega_i)\rangle$ can be monitored on a low-intensity subpicosecond time scale. Preliminary femtosecond results for conjugated polymers based upon nonlinear fluorescence mixing have been given by us in a very recent publication.[29]

(iii) The overall time-domain profiles of Figures 1–7 generally deviate from the Kohlrausch–Williams–Watts (KWW) stretched exponential[30] meanwhile frequently used in polymer photophysics[5]

$$\langle p_D(t)\rangle = \langle p_D(0)\rangle \exp[-(t/\tau_D)^\beta] \qquad (V.1)$$

which can be easily verified by plotting log ln $\langle p_D(0)\rangle/\langle p_D(t)\rangle$ versus a log t scale. This is not surprising, since the KWW law is, in general, a theoretically sound result for random, infinite systems,[30,31] while the site ensemble in the present simulation has a *finite, nonrandom* arrangement. Note therefore that for high dilute aromatic chains the KWW functional form is a rather poor trial function and cannot reproduce fluorescence trapping data. Although a $1/r^6$ dependence for all transitions seems to be justified, despite the problematic D $\gg$ T regime in these systems, the statistical mechanical calculation of the macroscopic (δ-pulse) fluorescence decay is mathematically not tractable, due to the nonrandom site density, the correlation of sites, and the lack of appropriate analytical expressions in the pair approximation.[32] So the actual form of the trapping law in the single chain limit is still an elusive problem. In our opinion, the transient trapping data analysis of this system in terms of its *eigenvalues spectrum* $\langle\Phi(\omega_i)\rangle$ is an essentially more unbiased procedure which does not require the knowledge of analytical time-domain trial functions. The result of such an analysis based upon simulated input spectra and synthetic data is given below.

(iv) In Figure 8a $\langle\Phi_D(\omega_i)\rangle$ provides an illustrative phenomenological platform for understanding the nature of reversible traps. The change of spectra with increasing detrapping parameter $q = \eta_0^{TD}/\eta_0^{DT}$ [Figure 8a (B)–(D)] shows a systematic trend to a narrow bimodal pattern, but note that $\langle\Phi_D(\omega_i)\rangle$, again, remains finite and cannot degenerate to the biexponential Birks limit[21] due to the finite volume property of the polymer. From the results of these simulations, we conjecture that even in reversible systems $\langle p_D(t)\rangle$ decays nonexponentially in migrational trapping experiments; multiexponential fits as usually applied in fluorescence reconvolution routines thus average

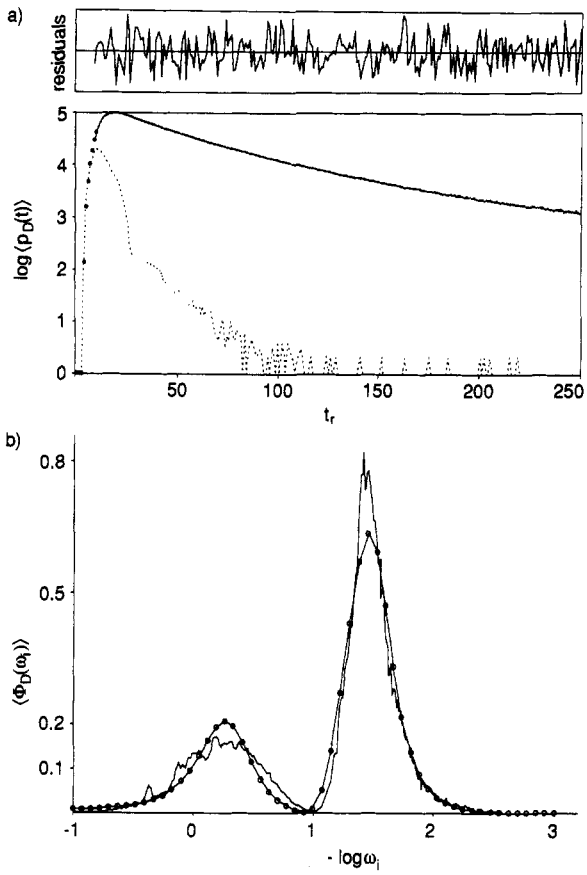

Figure 10. (a) Synthetic fluorescence convolution, according to $\mathbf{CL}\langle\Phi_D(\omega_i)\rangle = \mathbf{H}$ with input spectrum $\langle\Phi_D(\omega_i)\rangle$ from Figure 9a (C) (10^6 counts in the peak channel, normalized time scale): (dots) convolution data; (dashed profile) instrumental response. The solid curve through the data is best ESM fit with 50 exponentials ($\chi^2 = 1,002$). (b) Results of ESM recovery in $\log(1/\omega_i)$ space. The noisy pattern is with $\langle\Phi_D(\omega_i)\rangle$ from Figure 9a (C); the dotted pattern interpolated by the solid line is the reconstructed pattern of $\langle\Phi_D(\omega_i)\rangle$ (regularization parameter $\gamma = 10$). For details, see ref 12.

over distributions,[5] thereby producing simple curve parameterization that falsifies the background physics.

V.1. Some Remarks on the Reconstruction of $\langle\Phi(\omega_i)\rangle$. To close this work, a short comment concerning the feasibility for reconstructing the eigenvalues spectrum $\langle\Phi(\omega_i)\rangle$ from experimental fluorescence decay data appears in order. Since a fluorescence real-data profile $H(t)$ is a (discrete) one-sided convolution of the δ-pulse fluorescence response $F(t)$ with the laser instrumental impulse function $I(t)$, $H = I*F$, and $F(t)$ is proportional to the survival function $\langle p(t)\rangle$, according to $F(t) \propto \langle p(t)\rangle = \mathbf{L}\langle\Phi(\omega_i)\rangle$ (eq III.16), $\langle\Phi(\omega_i)\rangle$ is buried in the $H(t)$ pattern and effectively smoothed by both the Laplace transform and the convolution integral operator $\mathbf{C}$: $H(t) = \mathbf{CL}\langle\Phi(\omega_i)\rangle$. A central issue of the above $\langle\Phi(\omega_i)\rangle$ simulations in conjunction with time-resolved fluorescence experiments is therefore to solve the inverse problem $\mathbf{L}^{-1}\mathbf{C}^{-1}H(t) \rightarrow \langle\Phi(\omega_i)\rangle$ to draw conclusions about the underlying spectrum of hopping modes $\langle\Phi(\omega_i)\rangle$ in experimental systems.

Despite the severe ill-posedness of the problem,[33] unbiased numerical methods that extract distributions of states from the raw data have received, therefore, considerable attention in the analysis of (nonexponential) polymer fluorescence. Both the exponential series method (ESM)[34] and the maximum entropy method (MEM)[35,36] have yielded quite satisfactory results in the reconstruction of distributions of exponentials.[37,38] In particular, a regularized ESM algorithm[39] has shown a remarkable stability both in synthetic data back-and-forth simulations[40] and in experimental data analysis.[41]

A well-behaved example of numerical fluorescence data inversion obtained from this algorithm is given in Figure 10. (a) represents the synthetic data profile based upon the eigenvalue spectrum in Figure 9, (C) convoluted with an instrumental response. (b) shows the result of $\langle\Phi(\omega_i)\rangle$ reconstruction. For details, see the caption of Figure 10. A complete strategy of simulating a polymer fluorescence trapping experiment, including computation of $\langle\Phi(\omega_i)\rangle$, fluorescence convolution data synthesis, and the numerical reconstruction of $\langle\Phi(\omega_i)\rangle$ by regularization[39] has been given by us, very recently.[12,13] For quasi-continuous spectra the method provides a powerful fitting procedure and really makes sense in terms of configurational average of the lifetime spectrum; i.e., in a wider connotation, ESM or MEM results can map out the spatial chromophore distribution in a polymer. Thus both the $\langle\Phi(\omega_i)\rangle$ simulation and its reconstruction from noisy fluorescence data develop a deeper understanding of how the analysis of polymer fluorescence has to be devised. In principle, these numerical methods combined with polymer fluorescence data at a high level of precision and time resolution should stimulate future work on the analysis of concealed hopping mode distributions in polymers and related soft-condensed systems.

Acknowledgment. This work has been supported by the Austrian Fonds zur Förderung der wissenschaftlichen Forschung (FWF), Wien Austria (Project P 8775-PHY), which is gratefully acknowledged.

References and Notes

(1) Sperling, L. H. *Introduction to Physical Polymer Science*; Wiley-Interscience: New York, 1986.
(2) Bässler, H. *Phys. Status Solidi B* **1981**, *107*, 9.
(3) Kauffmann, H. F.; Weixelbaumer, W. D.; Bürbaumer, J.; Mollay, B. In *Photophysics of Polymers*; Hoyle, C. E., Torkelson, J. M., Eds.; ACS Symposium Series 358, American Chemical Society: Washington, DC, 1987.
(4) For example: Fitzgibbon, P. D.; Frank, C. W. *Macromolecules* **1982**, *15*, 733. Semerak, S. N.; Frank, C. W. *Adv. Polym. Sci.* **1984**, *54*, 33. Bässler, H. In *Hopping and Related Phenomena*; Fritsche H., Pollak M., Eds.; World Scientific: Singapore, 1990.
(5) Kauffmann, H. F. In *Photochemistry and Photophysics*; Rabek, J. F., Ed.; Chemical Rubber: Boca Raton, FL, 1990; Vol. 2.
(6) Fredrickson, G. H.; Andersen, H. C.; Frank, C. W. *Macromolecules* **1983**, *16*, 1456; **1984**, *17*, 54; **1984**, *17*, 1496.
(7) Ediger, M. D.; Fayer, M. D. *J. Chem. Phys.* **1983**, *78*, 2518; *Macromolecules* **1983**, *16*, 1839. Ediger, M. D.; Fayer, M. D. *J. Phys. Chem.* **1984**, *88*, 6108.
(8) Ediger, M. D.; Domingue, R. P.; Peterson, K. A.; Fayer, M. D. *Macromolecules* **1985**, *18*, 1182.
(9) Blumen, A.; Manz, J. *J. Chem. Phys.* **1979**, *71*, 4694. Huber, D. L.; Hamilton, D. S.; Barnett, B. *Phys. Rev. B* **1977**, *16*, 4642. Ching, W. Y.; Huber, D. L.; Barnett, B. *Ibid.* **1978**, *17*, 5025.
(10) Peterson, K. A.; Fayer, M. D. *J. Chem. Phys.* **1986**, *85*, 4702.
(11) Peterson, K. A.; Zimmt, M. B.; Linse, S.; Domingue, R. P.; Fayer, M. D. *Macromolecules* **1987**, *20*, 168. Peterson, K. A.; Stein, A. D.; Fayer, M. D. *Ibid.* **1990**, *23*, 111.
(12) Mollay, B.; Kauffmann, H. F. *Chem. Phys.* **1993**, *177*, 645.
(13) Mollay, B.; Kauffmann, H. F. In *Disorder Effects on Relaxational Processes*; Richert, R., Blumen, A., Eds.; Springer: Berlin, 1994; p 509.
(14) Byers, J. D.; Friedrich, M. S.; Friesner, R. A.; Webber, S. E. *Macromolecules* **1988**, *21*, 3402.
(15) Byers, J. D.; Parsons, W. S.; Friesner, R. A.; Webber, S. E. *Macromolecules* **1990**, *23*, 4835.
(16) Nauts, A.; Wyatt, R. E. *Phys. Rev. A* **1984**, *30*, 872. Wyatt, R. E. *Adv. Chem. Phys.* **1989**, *73*, 231.
(17) Binder, K.; Heermann, D. W. *Monte Carlo Simulation in Statistical Physics—An Introduction*; Springer: New York, 1988. Kremer, K.; Binder, K. *Comput. Phys. Rept. S* **1988**, *7*, 259.
(18) Press, W. H.; Flannery, B. P.; Teukolsky, S. A.; Vetterling, W. T. *Numerical Recipes, The Art of Scientific Computing*; Cambridge University Press: Cambridge, 1986.

(19) Förster, T. *Z. Naturforsch. A* **1949**, *4*, 321.
(20) Byers, J. D.; Parsons, W. S.; Webber, S. E. *Macromolecules* **1992**, *25*, 5935.
(21) Mollay, B. Thesis, Universität Wien, 1994.
(22) Birks, J. B. *Photophysics of Aromatic Molecules*; Wiley-Interscience: New York, 1970; Chapter 7. Birks, J. B.; Dyson, D. J.; Munro, I. H. *Proc. R. Soc. London Ser. A* **1963**, *275*, 575.
(23) Kauffmann, H. F.; Weixelbaumer, W. D.; Bürbaumer, J.; Schmoltner, A. M.; Olaj, O. F. *Macromolecules* **1985**, *18*, 104.
(24) Weixelbaumer, W. D.; Bürbaumer, J.; Kauffmann, H. F. *J. Chem. Phys.* **1985**, *83*, 1980.
(25) Mollay, B.; Landl, G.; Kauffmann, H. F. *J. Chem. Phys.* **1989**, *91*, 3744.
(26) Sienicki, K.; Winnik, M. A. *J. Chem. Phys.* **1987**, *87*, 2766. Sienicki, K.; Durocher, G. *Ibid.* **1991**, *94*, 6590.
(27) Marcus, A. H.; Diachun, N. A.; Fayer, M. D. *Macromolecules* **1993**, *26*, 3041.
(28) Shah, J. *IEEE J. Quantum Electron.* **1988**, *24*, 276. Mahr, H.; Hirsch, M. D. *Opt. Commun.* **1975**, *13*, 96.
(29) Mollay, B.; Lemmer, U.; Kersting, R.; Mahrt, R. F.; Kurz, H.; Kauffmann, H. F.; Bässler, H. *Phys. Rev. B*, in press.
(30) Williams, G. *Adv. Polym. Sci.* **1979**, *33*, 59.
(31) Blumen, A.; Manz, J. *J. Chem. Phys.* **1979**, *71*, 4694. Klafter, J.; Blumen, A. *Chem. Phys. Lett.* **1985**, *119*, 377. Mollay, B.; Kauffmann, H. F. *J. Chem. Phys.* **1992**, *97*, 4380.
(32) Klafter, J.; Blumen, A. *J. Chem. Phys.* **1984**, *80*, 875. Palmer, R. G.; Stein, D. L.; Abrahams, E.; Anderson, P. W. *Phys. Rev. Lett.* **1984**, *53*, 953. Blumen, A.; Zumofen, G.; Klafter, J. *Phys. Rev. B* **1984**, *30*, 5379.
(33) Tikhonov, A.; Arsenin, V. *Solutions of Ill-Posed Problems*; J. Wiley: New York, 1977. *Inverse and Ill-Posed Problems*; Engl, H. W., Groetsch, C. W., Eds.; Academic: Orlando, FL, 1987.
(34) James, D. R.; Ware, W. R. *Chem. Phys. Lett.* **1986**, *126*, 7. Siemarczuk, A.; Ware, W. R. *J. Phys. Chem.* **1987**, *91*, 3677; **1989**, *93*, 7609.
(35) Livesey, A. K.; Brochon, J.-C. *Biophys. J.* **1987**, *52*, 693.
(36) Landl, G. On the Convergence of the Maximum Entropy Method. Thesis, Johannes-Kepler-Universität, Linz, Austria, 1992.
(37) Siemarczuk, A.; Wagner, B. D.; Ware, W. R. *J. Phys. Chem.* **1990**, *94*, 1661.
(38) Brochon, J.-C.; Merola, F.; Livesey, A. K. In *Synchrotron Radiation and Dynamics Phenomena*; Beswick, A., Ed.; Conference Proceedings; American Institute of Physics: New York, 1992; Vol. 258, pp 435.
(39) Landl, G.; Langthaler, T.; Engl, H. W.; Kauffmann, H. F. *J. Comput. Phys.* **1991**, *95*, 1.
(40) Kauffmann, H. F.; Landl, G.; Engl, H. W. In *Large-Scale Molecular Systems: Quantum and Stochastic Aspects. Beyond the simple molecular picture*; Blumen, A., Gans, W., Amann, A., Eds.; NATO ASI Series B; Plenum: New York, 1991; Vol. 258, p 503.
(41) Kungl, A. J.; Landl, G.; Visser, A. J. W. G.; Breitenbach, M.; Kauffmann, H. F. *J. Fluorescence* **1992**, *2*, 63. Prenner, E.; Hermetter, A.; Landl, G.; Stütz, H.; Kauffmann, H. F.; Kungl, A. J. *J. Phys. Chem.* **1993**, *97*, 2788.